PHOTONICS Research

Spin-selective corner reflector for retro-reflection and absorption by a circular dichroitic manner

He Wang,[1,2,†] Yao Jing,[1,†] Yongfeng Li,[1,3,4] Lingling Huang,[2,*] Maochang Feng,[1] Qi Yuan,[1] Jiafu Wang,[1] Jieqiu Zhang,[1] and Shaobo Qu[1]

[1]Department of Basic Sciences, Air Force Engineering University, Xi'an 710051, China
[2]School of Optics and Photonics, Beijing Institute of Technology, Beijing 100081, China
[3]State Key Laboratory of Millimeter Waves, Southeast University, Nanjing 210096, China
[4]e-mail: liyf217130@126.com
*Corresponding author: huanglingling@bit.edu.cn

Received 11 February 2021; accepted 21 February 2021; posted 22 February 2021 (Doc. ID 422509); published 26 April 2021

Recently, we have witnessed an extraordinary spurt in attention toward manipulating electromagnetic waves by metasurfaces. Particularly, tailoring of circular polarization has attracted great amounts of interest in both microwave and optics regimes. Circular dichroism, an exotic chiroptical effect of natural molecules, has aroused discussion about this issue, yet it is still in its infancy. Herein, we initiate circular dichroism followed by controlling spin-selective wavefronts via chiral metasurfaces. An N-shaped chiral resonator loaded with two lumped resistors is proposed as the meta-atom producing an adequate phase gradient. Assisted by the ohmic dissipation of the introduced resistors, the effect of differential absorption provides an auxiliary degree of freedom for developing circularly polarized waves with a designated spin state. A planar corner reflector that can achieve retro-reflection and absorption for right- and left-handed circularly polarized incidence is theoretically simulated and experimentally observed at microwave frequency. Thus, our effort provides an alternative approach to tailoring electromagnetic waves in a circular dichroitic manner and may also find applications in multi-functional systems in optics and microwave regimes.

https://doi.org/10.1364/PRJ.422509

1. INTRODUCTION

Guiding of electromagnetic waves in a desired direction has captured the interest of researchers in both academic and engineering communities [1–4]. Metasurfaces, consisting of meticulously arranged sub-wavelength resonators, are examined to push the development of electromagnetic manipulation [2] and extensively applied to obtain unique phenomena such as anomalous reflection/refraction [5–7], vortex beam generation [8,9], beam splitting [10–12], and cloaking [13], among others, owing to their advantages of negligible thickness and high in-plane flexibility. In particular, the study of tailoring circularly polarized waves based on a metasurface platform prevents the bulky size of traditional optical devices. Thus, metasurfaces were widely utilized in the fields of polarimetry [14], circular polarizers [15], and spin-to-orbital converters [16,17]. However, because of the innate phase difference between distinct spin states, inverse phase profile flipping is acquired by shifting the polarization state of the incident waves. For example, wavefronts equivalent to convex and concave lenses can be achieved by spatial parabolic phase distribution under normal incidence of left-handed circularly polarized (LHCP)/right-handed circularly polarized (RHCP) waves and RHCP (LHCP) waves [18], respectively. With the help of the Pancharatnam–Berry phases, a large number of anisotropic and chiral metasurfaces are used to design spin-dependent meta-devices with distinct phase profiles [19–21]. Nevertheless, the manipulation of circularly polarized waves is not limited to this aspect. The immense potential in spin-selective techniques lies in chiral structures.

Chirality is a concept originating in biochemistry that is nearly omnipresent in nature and refers to a structure lacking a mirror symmetry plane [22]. In the context of microwave and optics regimes, chirality represents a series of unusual chiroptical responses that are significant in the fields of physics and material sciences [23–25], one such being circular dichroism. Owing to the characteristic of differential absorption of distinct spin states, circular dichroism provides an auxiliary degree of freedom for tailoring circularly polarized waves with designated spin states [26–28]. Unfortunately, it is not easily observed in nature owing to a mismatch between the scale of molecules and wavelength of incident light that considerably limits its practical applications in engineering [29].

Circular dichroism can be theoretically demonstrated via metasurfaces in an arbitrary span of frequency ranging from

the microwave to visible domain because of the deep subwavelength scale of meta-atoms or unit cells [30]. The methods of applying chiral nanoantenna [31,32], achiral oriented arrays [33], and multi-layered structures [34] are studied in optics and terahertz domains. Some investigations were conducted in the microwave frequency range as well, such as asymmetric split-ring resonators [35] and double-ring unit cells [22]. However, the mechanism in these works is governed by the symmetry-breaking substrate effect; thus the resulting circular dichroism was relatively weak. It is noticed that the conspicuous circular dichroism is significant for multi-dimensional electromagnetic manipulation in spin-selective systems, but research on this issue is still in the nascent stage.

In this work, we propose a paradigm for exhibiting distinct circular dichroism and shaping spin-selective wavefronts to push the development on this aspect. Ohmic dissipation into the two-dimensional (2D) structures is introduced to enhance the chiroptical responses. Two lumped resistors of 200 Ω each are loaded in an N-shaped chiral resonator that serves as the meta-atom of our design. Consequently, the Pancharatnam–Berry phases are combined with the spin-selective amplitude flipping from nearly 0 and 1 for distinct circular polarization states. As a proof-of-concept, we fabricate a planar dihedral corner reflector that achieves retro-reflection and absorption for RHCP and LHCP waves, respectively. The enhancement and reduction of the radar cross section (RCS) are simultaneously achieved by flipping the circular polarization states. Numerical simulations, as well as experimental measurements, are performed to verify the feasibility of the proposed paradigm.

2. DESIGN AND RESULTS

An illustration of the chiral metasurface-based dihedral corner reflector with appropriate phase gradients is presented in Fig. 1. Under the illumination of RHCP waves, the proposed corner reflector can reflect electromagnetic wave propagating back along its incident direction. Owing to its symmetric structure, there is a mono-static enhancement of the RCS in the 2D cutting-plane of the *xoz*-plane. In contrast, there is

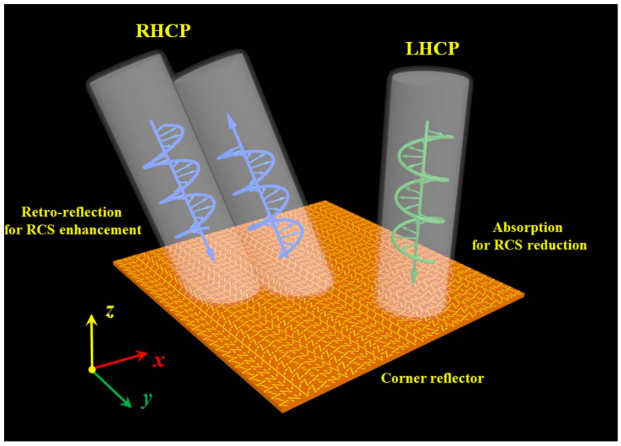

Fig. 1. Conceptual illustration of the proposed corner reflector. The functionality of retro-reflection for RCS enhancement and absorption for RCS reduction is achieved by flipping the polarization states of RHCP and LHCP waves, respectively.

electromagnetic absorption when the corner reflector is impinged upon by LHCP waves with reduction in the RCS. In sharp contrast to the traditional spin-dependent metasurfaces achieving different functionalities by the inverse phase profiles of distinct polarization states, the proposed scheme of applying circular dichroism provides another dimensional manipulation of amplitude flipping that presents an asymmetric propagation with spin-selective characteristics. Therefore, multi-dimensional manipulation of electromagnetic waves for phase, amplitude, and designated spin states can be achieved. In this design, electromagnetic absorption of LHCP waves is applied to achieve an almost omnidirectional RCS reduction instead of the diffusion-based approaches for only backward RCS reduction; this effectively prevents the scattering of energy in undesired directions.

To validate the operating principle of our design and explain it in detail, the underlying mechanism of achieving circular dichroism is analyzed by the Jones matrix. We assume that a circularly polarized wave of normal incidence propagates along the $-z$ direction and impinges on a desired reflective metasurface, of which the transmission amplitude can be regarded as 0. The electric field in the reflection region can be decomposed into two linearly polarized components in orthogonal directions [36]:

$$E_i = \frac{E_0}{\sqrt{2}} e^{ik_z z - i\omega t} \begin{pmatrix} \hat{x} & \hat{y} \end{pmatrix} \begin{pmatrix} 1 \\ \pm i \end{pmatrix}, \tag{1}$$

where "+" and "−" represent the RHCP and LHCP waves, respectively. Accordingly, the Jones matrix of the reflection fields is expressed as

$$E_r = R_{\text{lin}} E_i = \begin{pmatrix} r_{xx} & r_{xy} \\ r_{yx} & r_{yy} \end{pmatrix} E_i, \tag{2}$$

where R_{lin} is the reflection matrix under the Cartesian base; $r_{xx(yy)}$ and $r_{yx(yx)}$ are the co- and cross-polarized reflection coefficients under the incidence of x- and y-polarized waves, respectively. Furthermore, it is concluded that the reflection matrix for circular polarization is governed by eigenvectors $u = (1/2)^{1/2}(1, i)^T$ and $v = (1/2)^{1/2}(1, -i)^T$. In this work, the circular dichroism for total absorption of LHCP waves is analyzed as an example. With this aim, the reflection coefficients must satisfy $r_{LL} = r_{LR} = r_{RL} = 0$ and $r_{RR} = 1$. Thus, the solution is expressed by

$$R_{\text{lin}} = \frac{e^{i\gamma}}{2} \begin{pmatrix} 1 & i \\ i & -1 \end{pmatrix}, \tag{3}$$

where the polarization state is referred to the propagation direction of electromagnetic waves. The clockwise and counterclockwise directions are defined as RHCP and LHCP waves when viewed along the propagation direction, γ is an arbitrary phase shift, and a time-harmonic propagation of e^{-jwt} is considered. The eigenvalue of $\kappa = 0$ with the eigenvector of $(1, i)^T$ is obtained for the matrix R_{lin}, which indicates that total absorption of LHCP waves and reflection of RHCP waves with the handedness preserved are achieved.

It is concluded from the symmetry analysis that it is necessary to simultaneously break the n-fold rotational ($n > 2$) and mirror symmetries to achieve the circular dichroitic effect (see Appendix A). Based on this principle, an N-shaped meta-atom is proposed as a proof-of-concept to support our paradigm.

The topological structure of the proposed meta-atom is shown in Fig. 2(a), in which the N-shaped resonator is patched on a copper-backed F4B dielectric substrate of $\varepsilon_r = 2.65(1–0.001j)$. The N-shaped resonator is made of copper of electric conductivity 5.8×10^7 S/m^2. It is known that metasurface-based strategies of achieving circular dichroism originate from symmetry-breaking substrate effect or spin-dependent ohmic dissipation. In this design, lumped resistors are introduced to enhance the ohmic dissipation and exhibit strong chiral responses at microwave frequency. Two lumped resistors of 200 Ω each are loaded on the arms of the N-shaped resonator. The periodic length of the proposed meta-atom is set as $p = 5.20$ mm, height of the substrate is $d = 2.00$ mm, and thickness of the copper sheets is 0.02 mm. The structural parameters are optimized as $a = 0.70$ mm, $c = 0.72$ mm, $l = 5.00$ mm, and $w = 0.50$ mm.

To further elaborate the operating mechanism of the proposed meta-atom, the surface current is monitored by the computer simulation technology (CST) microwave studio. In the simulation, the boundary conditions along the x and y directions are set as the "unit cell" and two Floquet ports are fixed along the $\pm z$ directions. The surface current distributions at 20 GHz under the illumination of LHCP and RHCP waves are shown in Fig. 2(b). When circularly polarized waves are incident, the surface current is excited along the metallic resonator structure in a spin-selective manner; it was substantially suppressed when the LHCP waves impinged on the meta-atom, whereas it was highly enhanced under the illumination of RHCP waves. Therefore, it is inferred that different resonances are achieved under distinct polarization states, and this is attributed to the spin-selective ohmic dissipation introduced by the lumped resistors (circular dichroism is presented in Appendix B). The reflection amplitude of the meta-atom [Fig. 2(c)] shows the effect of differential absorption. Under normal incidence of the circularly polarized waves, the co-polarization reflection coefficient r_{RR} is >0.9 at 13–27 GHz, whereas r_{LL} was <0.2 in the same frequency band. The cross-polarization reflection coefficients r_{RL} and r_{LR} are both <0.2. In addition, the reflection characteristics for oblique incidence are discussed in Appendix B. It is indicated that the spin state of the RHCP reflection is converted with high efficiency, but the reflection of the LHCP wave is suppressed. In contrast to the metal plane, the proposed meta-atom can convert the spin states and preserve the handedness of the reflected waves. Thus, it is concluded that the proposed meta-atom is governed by the Pancharatnam–Berry phase ($\Phi = \pm 2\alpha$, where "+" and "–" represent RHCP and LHCP waves, respectively). Figure 2(d) illustrates the phase responses of the proposed meta-atom under the incidence of RHCP waves. A phase difference of approximately 60° is obtained at 18–30 GHz when the pivoting angle increases from 0° to 150° with an interval of 30°. Hence, the arbitrary forms of phase distribution can be theoretically acquired by meticulously aligning the meta-atoms owing to the high flexibility of phase manipulation.

Considering the preservation of handedness of the reflected waves and Pancharatnam–Berry phase of the proposed meta-atom, we design the planar dihedral corner reflector to achieve retro-reflection/absorption followed by the enhancement/reduction of the RCS. To achieve retro-reflection, an appropriate phase gradient is required. Therefore, we implement the generalized Snell's law [1]. When a flat metasurface is illuminated by a plane wave at an elevation angle of θ_i and azimuthal angle of φ_i, the direction of the reflected wave is calculated by [37]

$$\begin{cases} \theta_r = \arcsin \dfrac{\sqrt{(k_i \sin\theta_i \cos\varphi_i + \nabla\phi_x)^2 + (k_i \sin\theta_i \sin\varphi_i + \nabla\phi_y)^2}}{k_i} \\ \varphi_r = \arctan \dfrac{k_i \sin\theta_i \sin\varphi_i + \nabla\phi_y}{k_i \sin\theta_i \cos\varphi_i + \nabla\phi_x} \end{cases}, \quad (4)$$

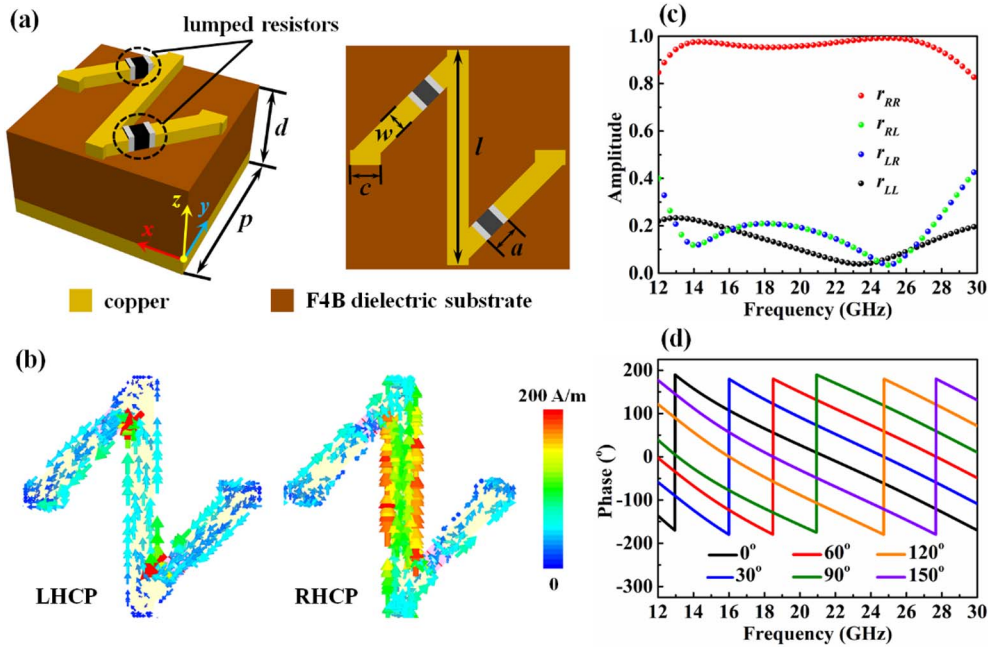

Fig. 2. (a) Topological structure of the proposed chiral meta-atom, (b) surface current distribution under the illumination of LHCP and RHCP waves, (c) co- and cross-polarization amplitudes $r_{RR(LL)}$ and $r_{RL(LR)}$ of the proposed meta-atom under normal incidence of circularly polarized waves, and (d) phase responses under the illumination of RHCP waves when the pivoting angle varies from 0° to 150° with an interval of 30°.

where k_i is the wave vector of the incident wave, $\nabla\phi_x$ and $\nabla\phi_y$ are the provided phase gradients along x- and y-axes, respectively. In this design, the propagation direction of the reflected wave is opposite to that of the incident wave. Therefore, $\nabla\phi_x$ and $\nabla\phi_y$ are set to meet the following conditions:

$$\begin{cases} \nabla\phi_x = 2k_i \sin\theta_i \cos\varphi_i \\ \nabla\phi_y = 2k_i \sin\theta_i \sin\varphi_i \end{cases}. \tag{5}$$

In accordance with Eq. (5), a dihedral corner reflector consisting of two parts with reverse phase gradients is proposed. The operating frequency is set at 20 GHz, and phase shift of each adjacent meta-atom was fixed as 94°. Consequently, retro-reflection is achieved when RHCP waves illuminated the corner reflector at an incident angle of ±22°. Hence, mono-static RCS enhancement is achieved in the angle ranges of $\theta = \pm 22°$. Owing to the effect of differential absorption, the reflection amplitude is nearly 0 when the polarization state flips to left-handed circular polarization. Thus, the effect of the phase gradient is inconspicuous, which infers an omnidirectional RCS reduction.

To verify the feasibility of our work, a planar corner reflector consisting of 30 × 30 meta-atoms of 156 mm × 156 mm in size is proposed. The required phase distribution, in accordance with the aforementioned theoretical calculation, is depicted in Fig. 3(a). Owing to the dihedral structure, the phase gradient is mirror symmetric in the transverse direction with respect to the y-axis. The schematic arrangement of meta-atoms is shown in Fig. 3(b). The pivoting step of the N-shaped resonator is fixed at 47° in the counter-clockwise direction to ensure the predesigned phase gradient, in keeping with the Pancharatnam–Berry phase. The finite difference time-domain technique is employed to investigate the far-field characteristics. All the boundary conditions along the x, y, and z directions are set as open (add space). In addition, the elevation angle of the incident wave is fixed as $\theta = 22°$. The three-dimensional (3D) far-field patterns under the illumination of RHCP and LHCP waves are compared in Fig. 3(c) wherein a clear circular dichroitic effect is observed. Retro-reflection is achieved under the illumination of RHCP waves whereas it is substantially suppressed when impinged upon by the LHCP waves. The normalized 2D far-field patterns at the cutting-plane of $\varphi = 0°$ are illustrated in Fig. 3(d), showing the far-field characteristics in the reflection region. A distinct reflected beam appears at $\theta = 22°$ in the xoz-plane for the RHCP wave, which is in good agreement with the theoretical prediction. On the other hand, the reflection of the LHCP wave is reduced by more than 12 dB in this direction. Furthermore, it is concluded that the distinct reflected beam of the RHCP wave emerged at −22° when the incident angle is −22° in terms of the dihedral phase distribution of the proposed corner reflector. Near-field performances are also monitored to further demonstrate the feasibility of our study. In Fig. 3(e), the electric field distributions of the E_x

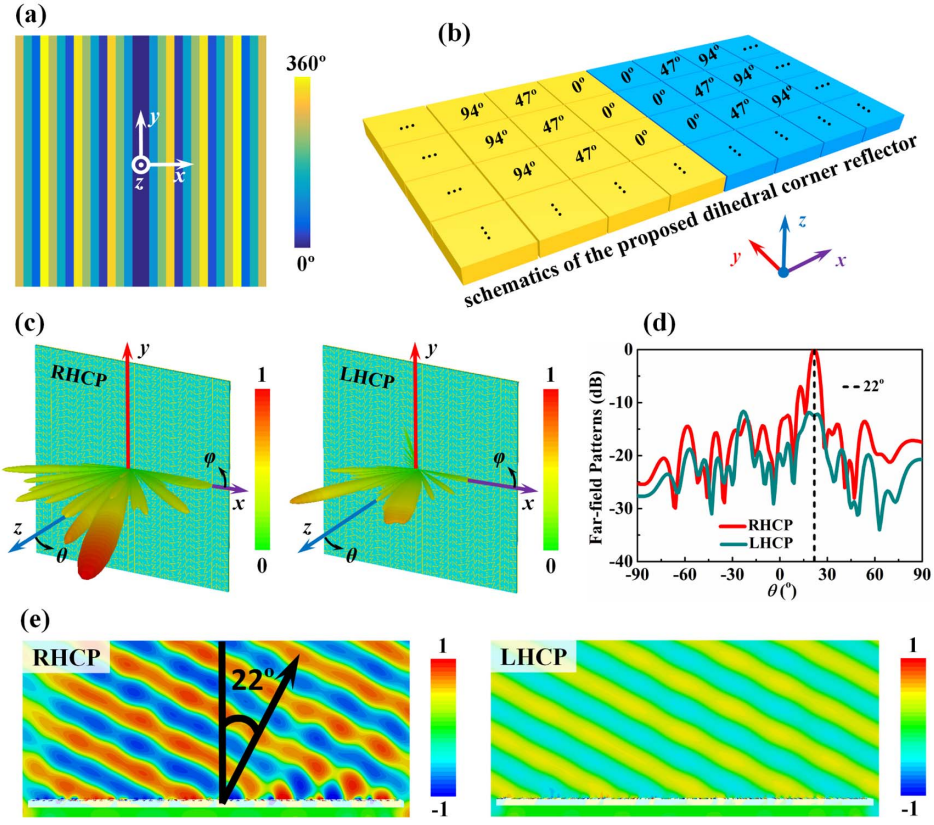

Fig. 3. (a) Phase distribution of the proposed planar corner reflector, (b) schematic of the arrangement of meta-atoms in the designed corner reflector, (c) 3D far-field patterns under the illumination of RHCP and LHCP waves at an incident angle of 22° at 20 GHz, (d) normalized 2D far-field patterns in the cutting-plane of $\varphi = 0°$, and (e) monitored electric field of E_x-component under the incidence of RHCP and LHCP waves at 20 GHz.

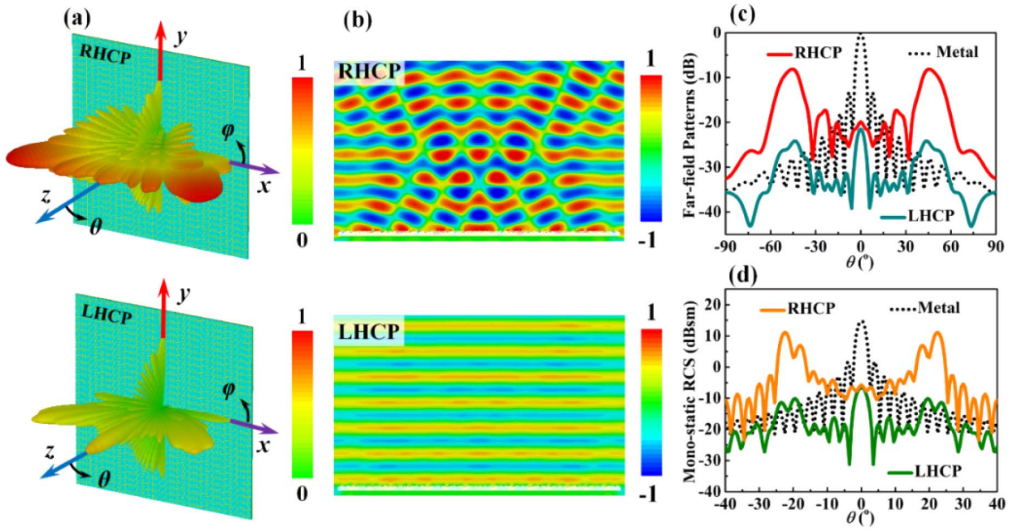

Fig. 4. (a) Simulated 3D far-field patterns under normal incidence of RHCP and LHCP waves at 20 GHz, (b) monitored electric field of E_x-component under the incidence of RHCP and LHCP waves at 20 GHz, (c) normalized 2D far-field patterns under normal incidence of RHCP and LHCP waves at the cutting-plane of the *xoz*-plane, and (d) simulated mono-static RCS with the elevation angle ranging from −40° to 40°.

component at 20 GHz in the reflection region are presented. The reflection field is along the reverse direction with respect to the incident RHCP waves, with an reflection angle of approximately 22°, which demonstrates adequate retro-reflection. The reflection field for LHCP waves is suppressed, indicating the circular dichroitic effect of the proposed corner reflector.

In addition, the far-field patterns under the illumination of waves at normal incidence are simulated. Figure 4(a) depicts the 3D far-field patterns at 20 GHz. It is observed that the energy of the reflected wave is distinctly enhanced in the case of incidence of the RHCP waves. However, the far-field pattern of the LHCP wave is considerably reduced. Moreover, the far-field patterns are symmetric along the *yoz*-plane owing to the symmetry of two opposite phase gradients. The normalized far-field patterns at the cutting-plane of *xoz*-plane are shown in Fig. 4(c). A metallic sheet of the same size as that of the proposed corner reflector is used for comparison; the direction of the reflected wave follows the classic reflection law indicating specular reflection. The electric field of the E_x component is monitored and is shown in Fig. 4(b). The enhancement and reduction of the electric field under the RHCP and LHCP waves are consistent with our prediction, verifying the circular dichroitic effect.

Moreover, the performance of mono-static RCS is simulated. The RCS curves in the cutting-plane of the *xoz*-plane with the elevation angle ranging from −40° to 40° are presented in Fig. 4(d). In contrast to the metallic sheet of the same scale, a distinct enhancement in the RCS is achieved in a wide angular range in the regions of approximately ±22° under the incidence of RHCP waves. The maximum value of RCS enhancement is 25 dB relative to the metallic sheet. According to the analysis, the mono-static RCS of LHCP waves is sharply reduced due to the circular dichroitic effect. The simulation results show that the RCS reduction is >20 dB for normal incidence. In addition, there are two small rises around the elevation angle of $\theta = \pm 22°$ attributed to a slight imperfection in the absorption of the LHCP wave.

To experimentally verify the proposed paradigm and demonstrate the enhancement/reduction of RCS, a metasurface prototype of size 156 mm × 156 mm is fabricated by using the printed circuit board technology. An F4B dielectric substrate coated with double-sided copper sheets is taken by the acid etching technique, metallic structures of N-shaped resonators are formed on one side; the other side is not etched, and the copper sheet is preserved. In the fabrication process, all the parameters are kept the same as in the simulations. The photograph of the prototype and a zoom view of the meta-atoms are depicted in Fig. 5(a), in which the lumped resistors are loaded in the predesigned position by welding technique. Chip fixed resistors of the type 1005 in metric expression are used. The experimental setup is placed in an anechoic chamber to prevent electromagnetic uncertainty in the environment (see Appendix C). The measurement of the mono-static RCS is carried out within the range from −40° to 40° of the elevation angle for verification.

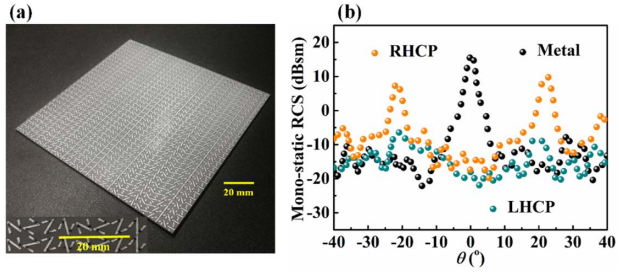

Fig. 5. (a) Photograph of the fabricated metasurface prototype with the inset showing the meta-atoms, and (b) measured mono-static RCS under the illumination of RHCP and LHCP waves at 20 GHz. The mono-static RCS of a metallic sheet of the same size as the proposed metasurface is shown for comparison.

The measured mono-static RCSs of the proposed corner reflector at 20 GHz and a metallic sheet of the same size under the illumination of RHCP and LHCP waves are compared and shown in Fig. 5(b). For the metallic sheet, the energy is concentrated in the backward direction owing to specular reflection. The maximum value of RCS occurs at nearly 0° but is weak in the other angular domains. In sharp contrast, the RCS curve of the proposed corner reflector shows two distinct peaks at ±22° under the incidence of RHCP waves, demonstrating the considerable RCS enhancement within this range. On the other hand, no distinct peak appears on the RCS curve when illuminated by LHCP waves. Moreover, the RCS in the range of elevation angle from −40° to 40° is < −10 dB, indicating that nearly omnidirectional RCS reduction is achieved. The measured results are in accordance with those obtained in the simulations, verifying the feasibility of our method. The slight deviations between the measured and simulated results can be attributed to the uncertainty in the welding of the resistors and unavoidable interference in the experimental environment.

3. CONCLUSIONS

In summary, we proposed a paradigm of tailoring circularly polarized waves in a dichroitic manner. A meta-atom that exhibits distinct circular dichroism is attained by introducing ohmic dissipation of a 2D chiral resonator through loading lumped resistors. Owing to the spin conversion characteristics of the meta-atom, a flexible manipulation of phase gradient is achieved by applying the Pancharatnam–Berry phase. The arbitrary form of the phase profile can be theoretically acquired for the designated circular polarization state. A dihedral corner reflector with symmetric phase gradients with respect to the *yoz*-plane is designed as a proof-of-concept. The simulation and measurement are conducted in the microwave regime that effectively demonstrates the feasibility of our method and manifestation of mono-static RCS enhancement/reduction for RHCP/LHCP waves. Significantly, the proposed paradigm provides an alternative approach to design spin-selective metadevices with an auxiliary dimension for tailoring electromagnetic waves that is suitable in circular polarization systems and radar/communication applications.

APPENDIX A: UNDERLYING MECHANISM OF ACHIEVING CIRCULAR DICHROISM

The cases of rotation and mirror symmetry are discussed as follows.

First, we consider the case of rotational symmetry. By rotating a chiral structure through an arbitrary angle, the new reflection matrix can be further explained by matrix transformation of rotation [38]:

$$R' = D_\alpha^{-1} R_{\text{lin}} D_\alpha, \quad \text{with} \quad D_\alpha = \begin{pmatrix} \cos\alpha & \sin\alpha \\ -\sin\alpha & \cos\alpha \end{pmatrix}, \tag{A1}$$

where α stands for the rotation angle of the new reflection matrix of R'. As the chiral structure possesses the rotational symmetry properties of α, the matrix transformation leads to $R' = R_{\text{lin}}$. Thus, the general condition for rotational symmetry is obtained as

$$\sin\alpha \begin{pmatrix} r_{xy} + r_{yx} & r_{yy} - r_{xx} \\ r_{yy} - r_{xx} & -r_{xy} - r_{yx} \end{pmatrix} = 0, \tag{A2}$$

and the solutions to simultaneously satisfy Eqs. (3) and (A2) are $\alpha = k\pi$, $k = 0, \pm 1, \pm 2, \ldots$ Hence, it is concluded that only the C_2 symmetric group can provide circular dichroism.

Next, suppose the mirror symmetry plane of a symmetric structure is rotated from the *xoz*-plane through a rotational angle of α with respect to the *z*-axis. Accordingly, the reflection matrix is expressed as

$$R'' = A_x^{-1} D_{-\alpha}^{-1} R_{\text{lin}} D_{-\alpha} A_x, \quad \text{with} \quad A_x = \begin{pmatrix} 1 & 0 \\ 0 & -1 \end{pmatrix}, \tag{A3}$$

where A_x is the mirror matrix with respect to the *x*-axis. According to the symmetry condition of $R'' = R_{\text{lin}}$, the solution is obtained as

$$\sin(2\alpha)(r_{xx} - r_{yy}) + 2\cos(2\alpha) r_{xy} = 0, \tag{A4}$$

where $(r_{xx} - r_{yy})/r_{xy}$ is a pure imaginary number so that the mirror symmetry structure has no solution for the corresponding matrix transformation. Therefore, circular dichroism cannot be attained in structures that exhibit mirror symmetry with respect to the incidence plane.

Therefore, to achieve the circular dichroitic effect, it is necessary to simultaneously break the *n*-fold rotational ($n > 2$) and mirror symmetries [37]. Based on this principle, we propose an N-shaped resonator as the meta-atom of our design.

APPENDIX B: CIRCULAR DICHROISM IN THE PROPOSED N-SHAPED META-ATOM

The curves of absorption of the RHCP/LHCP waves and corresponding circular dichroism are presented in Fig. 6(a). It is observed that the incident LHCP waves are absorbed to a great extent in the 12–30 GHz range; whereas the absorption of RHCP waves is <0.1 within the same frequency band. The circular dichroism is calculated by using $\text{CD} = A_{\text{LHCP}} - A_{\text{RHCP}}$; therefore, it is >0.6 in the 12–30 GHz range. Moreover, it is seen that circular dichroism >0.9 can be achieved in a wide frequency band from 14 GHz to 27 GHz, which indicates the distinctive performance of differential absorption and wideband characteristics. However, the variation of circular dichroism changes with the introduction of ohmic dissipation. As can be seen from Fig. 6(b), the circular dichroism of the proposed meta-atom increases with the enhancement of resistance in the operating frequency range. In this design, the resistance is optimized at 200 Ω to adapt the appropriate ohmic dissipation and thereafter exhibit a strong circular dichroitic effect for reflection of LHCP waves and absorption of RHCP waves.

Figure 6(c) shows the co-polarization amplitudes r_{RR} and r_{LL} for oblique incidence from 0° to 30°. Both r_{RR} and r_{LL} are stable at different angles of incidence. It is seen that the curves of r_{RR} are >0.90 and r_{LL} are <0.25, which indicates the circular dichroism of the proposed meta-atom under illumination by circularly polarized waves at different incident angles. In this work, an angle of incidence of $\theta = \pm 22°$ is applied. The reflection characteristics are shown in Fig. 6(d).

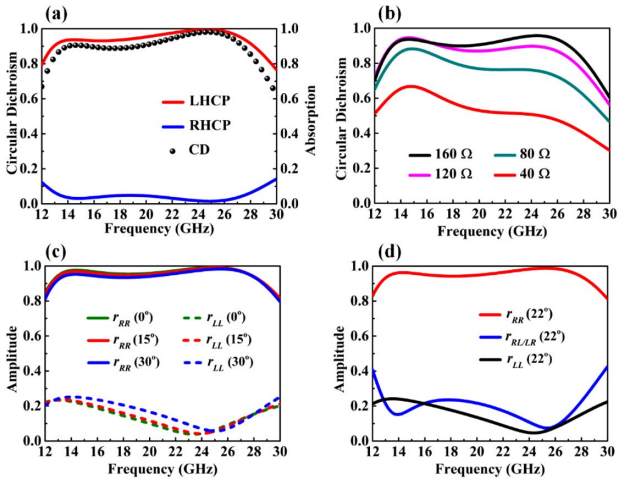

Fig. 6. (a) Curves of absorption and circular dichroism of the proposed N-shaped meta-atom, (b) curves of circular dichroism when the resistance increases from 40 Ω to 160 Ω, (c) co-polarization amplitudes r_{RR} and r_{LL} under oblique incidence from 0° to 30°, and (d) reflection curves under oblique incidence at an angle of 22°.

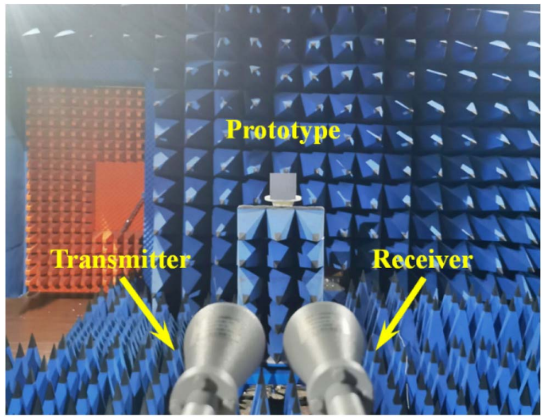

Fig. 7. Photograph of the experimental setup for the RCS measurement.

APPENDIX C: EXPERIMENTAL SETUP

A photograph of the experimental setup for the measurement of the RCS is shown in Fig. 7. The measurement was carried out in an anechoic chamber to reduce the electromagnetic uncertainty in the environment. The prototype was fixed on a turntable that could rotate through 360° in a horizontal plane. Two standard circularly polarized horn antennas were placed far enough from the prototype: one served as a transmitter and the other as a receiver. The two antennas were connected to the two ports of an Agilent N5224A vector network analyzer. During the measurement, the turntable rotated from −40° to 40° to obtain the RCS performance in this angle range.

Funding. Natural Science Foundation of Shaanxi Province (2020JM-342); Beijing Outstanding Young Scientist Program (BJJWZYJH01201910007022); National Natural Science Foundation of China (61775019, 61971435, 61971437).

Disclosures. The authors declare no conflicts of interest.

†These authors contributed equally to this work.

REFERENCES

1. N. Yu, P. Genevet, M. A. Kats, F. Aieta, J. Tetienne, F. Capasso, and Z. Gaburro, "Light propagation with phase discontinuities: generalized laws of reflection and refraction," Science **334**, 333–337 (2011).
2. N. Yu and F. Capasso, "Flat optics with designer metasurfaces," Nat. Mater. **13**, 139–150 (2014).
3. S. Chen, Z. Li, W. Liu, H. Cheng, and J. Tian, "From single-dimensional to multidimensional manipulation of optical waves with metasurfaces," Adv. Mater. **31**, 1802458 (2019).
4. Q. Ma and T. J. Cui, "Information metamaterials: bridging the physical world and digital world," PhotoniX **1**, 1 (2020).
5. S. Sun, K. Yang, C. Wang, T. Juan, W. T. Chen, C. Y. Liao, Q. He, S. Xiao, W. Kung, G. Guo, L. Zhou, and D. P. Tsai, "High-efficiency broadband anomalous reflection by gradient meta-surfaces," Nano Lett. **12**, 6223–6229 (2012).
6. Z. Li, E. Palacios, S. Butun, and K. Aydin, "Visible-frequency metasurfaces for broadband anomalous reflection and high-efficiency spectrum splitting," Nano Lett. **15**, 1615–1621 (2015).
7. N. K. Grady, J. E. Heyes, D. R. Chowdhury, Y. Zeng, M. T. Reiten, A. K. Azad, A. J. Taylor, D. A. R. Dalvit, and H. Chen, "Terahertz metamaterials for linear polarization conversion and anomalous refraction," Science **340**, 1304–1307 (2013).
8. S. Yu, L. Li, G. Shi, C. Zhu, and Y. Shi, "Generating multiple orbital angular momentum vortex beams using a metasurface in radio frequency domain," Appl. Phys. Lett. **108**, 241901 (2016).
9. Y. Bao, J. Ni, and C. Qiu, "A minimalist single-layer metasurface for arbitrary and full control of vector vortex beams," Adv. Mater. **32**, 1905659 (2019).
10. T. J. Cui, M. Q. Qi, X. Wan, J. Zhao, and Q. Cheng, "Coding metamaterials, digital metamaterials and programmable metamaterials," Light Sci. Appl. **3**, e218 (2014).
11. T. Cui, S. Liu, and L. Li, "Information entropy of coding metasurface," Light Sci. Appl. **5**, e16172 (2016).
12. H. Xu, L. Zhang, Y. Kim, G. Wang, X. Zhang, Y. Sun, X. Ling, H. Liu, Z. Chen, and C. Qiu, "Wavenumber-splitting metasurfaces achieve multichannel diffusive invisibility," Adv. Opt. Mater. **6**, 1800010 (2018).
13. Z. H. Jiang, P. E. Sieber, L. Kang, and D. H. Werner, "Restoring intrinsic properties of electromagnetic radiators using ultralightweight integrated metasurface cloaks," Adv. Funct. Mater. **25**, 4708–4716 (2015).
14. A. Ehsan, K. S. Mahsa, A. Amir, and F. Andrei, "Full stokes imaging polarimetry using dielectric metasurfaces," ACS Photon. **5**, 3132–3140 (2018).
15. J. K. Gansel, M. Thiel, M. S. Rill, M. Decker, K. Bade, V. Saile, F. G. Von, S. Linden, and M. Wegener, "Gold helix photonic metamaterial as broadband circular polarizer," Science **325**, 1513–1515 (2009).
16. Y. Guo, M. Pu, Z. Zhao, Y. Wang, J. Jin, P. Gao, X. Li, X. Ma, and X. Luo, "Merging geometric phase and plasmon retardation phase in continuously shaped metasurfaces for arbitrary orbital angular momentum generation," ACS Photon. **3**, 2022–2029 (2016).
17. H. Wang, Y. Li, H. Chen, Y. Shen, J. Wang, J. Zhang, A. Zhang, T. Cui, and S. Qu, "Spin-to-orbital angular momentum conversion with quasi-continuous spatial phase response," Adv. Opt. Mater. **7**, 1901188 (2019).
18. L. Huang, X. Chen, B. Bai, Q. Tan, G. Jin, T. Zentgraf, and S. Zhang, "Helicity dependent directional surface plasmon polariton excitation using a metasurface with interfacial phase discontinuity," Light Sci. Appl. **2**, e70 (2013).
19. T. Cai, G. Wang, H. Xu, S. Tang, H. Li, J. Liang, and Y. Zhuang, "Bifunctional Pancharatnam–Berry metasurface with high-efficiency helicity-dependent transmissions and reflections," Ann. Phys. **530**, 1700321 (2017).

20. H. Wang, J. Du, H. Wang, Y. Lu, and P. Wang, "Generation of spin-dependent accelerating beam with geometric metasurface," Adv. Opt. Mater. **7**, 1900552 (2019).
21. W. Guo, G. Wang, X. Luo, H. Hou, K. Chen, and Y. Feng, "Ultrawideband spin-decoupled coding metasurface for independent dual-channel wavefront tailoring," Ann. Phys. **532**, 1900472 (2020).
22. L. Jing, Z. Wang, Y. Yang, B. Zheng, Y. Liu, and H. Chen, "Chiral metamirrors for broadband spin-selective absorption," Appl. Phys. Lett. **110**, 231103 (2017).
23. M. Khorasaninejad, W. T. Chen, A. Y. Zhu, J. Oh, R. C. Devlin, D. Rousso, and F. Capasso, "Multispectral chiral imaging with a metalens," Nano Lett. **16**, 4595–4600 (2016).
24. S. Zhang, J. Zhou, Y. Park, J. Rho, R. Singh, S. Nam, A. K. Azad, H. Chen, X. Yin, A. J. Taylor, and X. Zhang, "Photoinduced handedness switching in terahertz chiral metamolecules," Nat. Commun. **3**, 942 (2012).
25. Y. Chen, X. Yang, and J. Gao, "Spin-controlled wavefront shaping with plasmonic chiral geometric metasurfaces," Light Sci. Appl. **7**, 84 (2018).
26. H. Xu, G. Hu, Y. Li, L. Han, J. Zhao, Y. Sun, F. Yuan, G. Wang, Z. H. Jiang, X. Ling, T. J. Cui, and C. Qiu, "Interference-assisted kaleidoscopic meta-plexer for arbitrary spin-wavefront manipulation," Light Sci. Appl. **8**, 3 (2019).
27. S. Yang, Z. Liu, S. Hu, A. Jin, H. Yang, S. Zhang, J. Li, and C. Gu, "Spin-selective transmission in chiral folded metasurfaces," Nano Lett. **19**, 3432–3439 (2019).
28. Q. Wang, E. Plum, Q. Yang, X. Zhang, Q. Xu, Y. Xu, J. Han, and W. Zhang, "Reflective chiral meta-holography: multiplexing holograms for circularly polarized waves," Light Sci. Appl. **7**, 25 (2018).
29. L. Jing, Z. Wang, R. Maturi, B. Zheng, H. Wang, Y. Yang, L. Shen, R. Hao, W. Yin, E. Li, and H. Chen, "Gradient chiral metamirrors for spin-selective anomalous reflection," Laser Photon. Rev. **11**, 1700115 (2017).
30. M. Feng, X. Chen, Y. Li, Q. Zheng, Y. Han, J. Zhang, J. Wang, Y. Hou, Z. Liu, X. Li, C. Wang, J. Jing, H. Ma, and S. Qu, "Circularly polarized spin-selectivity absorbing coding phase gradient metasurface for RCS reduction," Adv. Theor. Simul. **3**, 1900217 (2020).
31. M. Hentschel, M. Schäferling, B. Metzger, and H. Giessen, "Plasmonic diastereomers: adding up chiral centers," Nano Lett. **13**, 600–606 (2013).
32. T. Fu, Y. Qu, T. Wang, G. Wang, Y. Wang, H. Li, J. Li, L. Wang, and Z. Zhang, "Tunable chiroptical response of chiral plasmonic nanostructures fabricated with chiral templates through oblique angle deposition," J. Phys. Chem. C **121**, 1299–1304 (2017).
33. B. M. Maoz, A. B. Moshe, D. Vestler, O. Bar-Elli, and G. Markovich, "Chiroptical effects in planar achiral plasmonic oriented nanohole arrays," Nano Lett. **12**, 2357–2361 (2012).
34. Y. Svirko, N. Zheludev, and M. Osipov, "Layered chiral metallic microstructures with inductive coupling," Appl. Phys. Lett. **78**, 498–500 (2001).
35. E. Plum and N. I. Zheludev, "Chiral mirrors," Appl. Phys. Lett. **106**, 221901 (2015).
36. C. Menzel, C. Rockstuhl, and F. Lederer, "Advanced Jones calculus for the classification of periodic metamaterials," Phys. Rev. A **82**, 053811 (2010).
37. M. Feng, Y. Li, J. Zhang, Y. Han, J. Wang, H. Ma, and S. Qu, "Wide-angle flat metasurface corner reflector," Appl. Phys. Lett. **113**, 143504 (2018).
38. Z. Wang, H. Jia, K. Yao, W. Cai, H. Chen, and Y. Liu, "Circular dichroism metamirror with near-perfect extinction," ACS Photon. **3**, 2096–2101 (2016).